Journal of Applied Polymer Science

Mechanical Properties and Thermostability of Polyimide/Mesoporous Silica Nanocomposite via Effectively Using the Pores

Xiangyuan Ye,[1,2] Jinqing Wang,[1] Ye Xu,[1,2] Lengyuan Niu,[1,2] Zengjie Fan,[1,2] Peiwei Gong,[1,2] Limin Ma,[1] Honggang Wang,[1] Zhigang Yang,[1] Shengrong Yang[1]

[1]State Key Laboratory of Solid Lubrication, Lanzhou Institute of Chemical Physics, Chinese Academy of Sciences, Lanzhou, 730000, People's Republic of China

[2]University of Chinese Academy of Sciences, Beijing, 100080, People's Republic of China

Correspondence to: J. Wang (E-mail: jqwang@licp.cas.cn) and H. Wang (E-mail: hgwang@licp.cas.cn)

ABSTRACT: Series of polyimide (PI)/mesoporous silica nanospheres (MSNs) nanocomposite films with different contents of MSNs were successfully prepared via a simple wet impregnation method. The morphologies, microstructures, mechanical properties, transmittance, and thermal properties of the prepared PI and the PI/MSNs nanocomposite films were investigated in detail. As a result, the thermal stability and mechanical performances of PI were obviously improved by incorporating MSNs into PI. The tensile stress and Young's modulus of the nanocomposite film with 5 wt % MSNs were raised up to 97.65 MPa and 2220.06 MPa, which are greatly higher than the values of 82.51 MPa and 1440.86 MPa for the pure PI film. Experimental results confirmed that the designed polymerization tactic, which occurred in the pores of the MSNs, facilitated to enhance the mechanical and physical performances of the PI/MSNs nanocomposite films, and definitely induced better integration between organic matrix and inorganic nanofillers. © 2014 Wiley Periodicals, Inc. J. Appl. Polym. Sci. **2014**, *131*, 41173.

KEYWORDS: composites; films; mechanical properties; polyimides; thermogravimetric analysis (TGA)

Received 5 March 2014; accepted 13 June 2014

DOI: 10.1002/app.41173

INTRODUCTION

Recently, organic–inorganic hybrid materials, as a new class of advanced materials, have attracted intensive research interest. These materials can be prepared or processed by using various inorganic nanofillers, which endowed materials tunable properties and promising applications in various fields.[1] Furthermore, the organic–inorganic hybrid materials offer the possibility of combining the advantages and overcoming the disadvantages of the two different components. As an important organic matrix, polyimide (PI) has attracted considerable attention due to its outstanding thermal and chemical stabilities, as well as good mechanical properties, etc. Therefore, it has been considered as one of the most important super-engineering materials and widely applied in the fields of microelectronics and aerospace industries.[2,3]

As the auxiliary component of organic–inorganic hybrid materials, the inorganic fillers play significant roles. Specially, the inorganic nanofillers were endowed with promising future in the field of composite materials as they have large surface areas, leading to a dramatic increase in interfacial area. Even at a very low amount of usage, these nanofillers can greatly improve the macroscopic properties of the polymers.[4–7] Some typical inorganic nanofillers, including carbon materials (such as carbon nanotubes, graphene nanosheets) and metal oxides (such as silica, titanium dioxide, alumina), etc.,[8–15] efficiently improved the properties of PI. Among these inorganic materials, silica has received much more attention in recent years because of its high thermal stability and extremely low thermal expansion coefficient (5×10^{-7} K^{-1}). In order to investigate the mechanical properties of strength and modulus, as well as the thermal stability of PI, kinds of silicas with different morphology (such as silica sphere, silica tube, etc.) have been employed to prepare PI/silica composite materials. The research results indicated that most of these nonporous silicas can effective improve the mechanical properties and thermal stability of PI.[16–31]

Compared with many works on PI/nonporous silica nanocomposites, the ones on PI/mesoporous silica nanocomposites are rarely referred to.[32–35] Actually, mesoporous silica with the unique pore structure also can reinvest PI with outstanding properties. For examples, Lin et al.[33] reported the preparation of PI composite films containing the SBA-15 or the SBA-16

Additional Supporting Information may be found in the online version of this article.

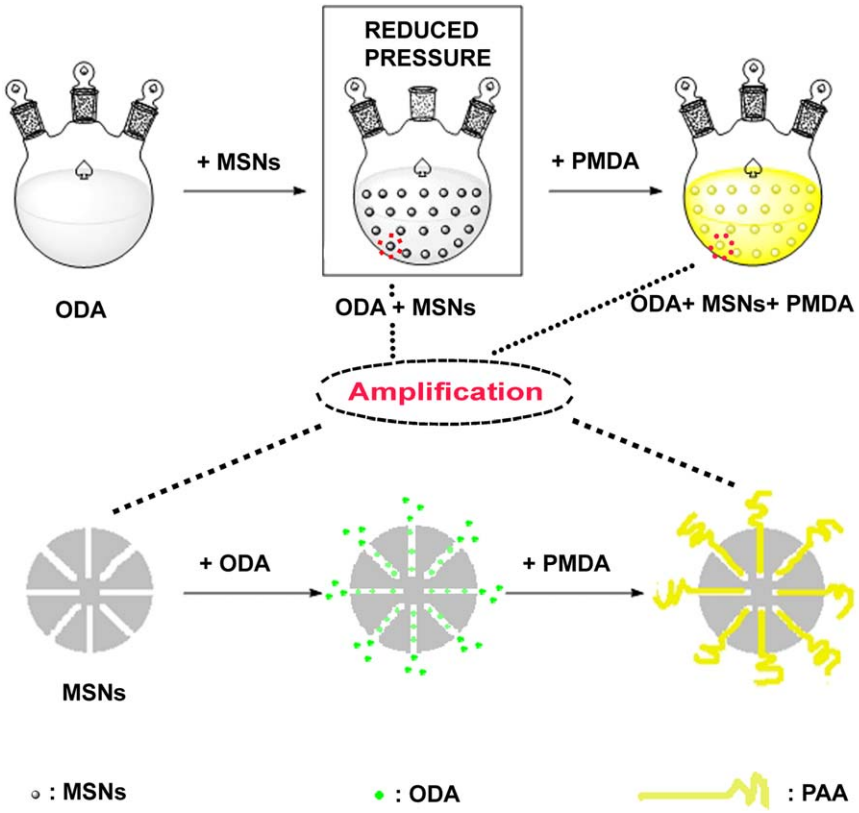

Scheme 1. Synthesis strategy for monomer polymerization in the pores of MSNs. [Color figure can be viewed in the online issue, which is available at wileyonlinelibrary.com.]

mesoporous silica modified with (γ-aminopropyl) triethoxysilane (APTS) via the in situ polymerization and the subsequent thermal imidization. This work indicated that the dielectric constants of the PI composite films can be reduced by incorporating SBA-15 or SBA-16. Similar results were also observed by Min et al.[34] In addition, Lee et al.[35] undertook the preparation and characterization of PI/mesoporous silica nanocomposite films in virtue of a water soluble poly(amic acid) (PAA) ammonium salt and the results revealed that tensile modulus of the hybrid nanocomposite films were lower than the pure PI although the dielectric constants of the composite films could be reduced through this method. These studies successfully took the advantages of the air voids ($k = 1$) stored within the mesoporous silica to reduce the dielectric constants of the pure PI.

From what have been discussed above, most of researchers paid attention to functionalize surface of mesoporous silica and kept the air volume stored within the mesoporous silica. However, the pores of mesoporous silica truly generated the large surface areas which can be beneficial to availably incorporate PI and mesoporous silica if the pores can be utilized effectively. In other words, previous pioneer works mainly focused on how to retain the air voids (in the pores of mesoporous silica) and finally decreased the dielectric constants; herein, we managed to take advantages of the pores of mesoporous silica to increase the contact area between PI and mesoporous silica, aiming at improving the mechanical properties and the thermostability of PI, and the similar works have not been reported by others. Specifically, a synthetic route toward PI/mesoporous silica nanospheres (MSNs) nanocomposite films has been developed through polymerization occurred on the surfaces and inside the pores of mesoporous silica. As shown in Scheme 1, 4,4′-oxydianiline (ODA) was infused into the pores of mesoporous silica via wet impregnation method, following the step that the second monomer of pyromellitic dianhydride (PMDA) was added into the reaction system to synthesize PAA. Finally, PI/MSNs nanocomposite films were successfully achieved through the final step of thermal imidization.

EXPERIMENTAL

Materials

PMDA, ODA, hexadecyltrimethylammonium bromide (CTAB), and tetraethoxysilane (TEOS) used as silica source were purchased from Sinopharm Chemical Reagent Company. *N,N′*-dimethylacetamide (DMAc) was obtained from Tianjin Chemical Reagent Company. All chemicals are of reagent quality and used as received.

Preparation of MSNs

The MSNs were prepared via a simple sol–gel process by using CTAB as a structure-directing agent and TEOS as the silica precursor. During preparation, aqueous sodium hydroxide (NaOH) was employed as base and strong stirring was performed to inhibit agglomeration of the formed beads. It has been demonstrated that the diameter of MSNs can be controlled by changing experimental conditions and adjusting molar ratio of CTAB

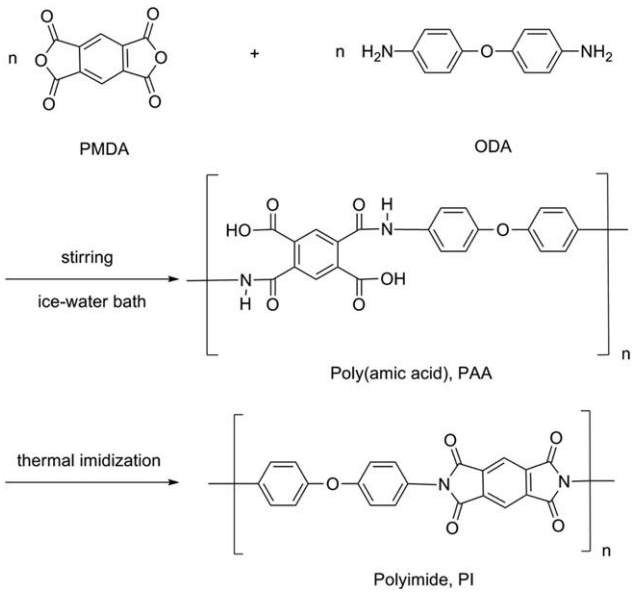

Figure 1. Two-step reaction scheme for synthesizing PMDA-ODA PI.

to TEOS following the previous reports.[36] A typical synthesis was described as follows: (1) 0.56 g NaOH was dissolved in the mixed solution of 900 mL ultrapure water and 100 mL ethanol by stirring; (2) 2.04 g CTAB was added into the solution with stirring at 80°C; (3) When the solution became homogeneous, 11.04 g TEOS was poured with stirring and then a white slurry was formed, followed being kept with stirring at 80°C for 2 h; (4) The resultant product was filtered, washed with ultrapure water, dried at 60°C at reduced pressure for 12 h, followed by calcination at 550°C in air for 5 h.[36]

Preparation of PAA/MSNs Nanoparticles and PI/MSNs Nanoparticles

To gain precise evidence on polymerization in the pores of MSNs, PAA/MSNs nanoparticles and PI/MSNs nanoparticles were, respectively, prepared. First, 30 mL DMAc and 2.0 g ODA were added into a three-necked flask with stirring and cooled in an ice-water bath. After the ODA was dissolved completely, about 0.25 g MSNs was dispersed in the solution with sonication for 60 min, the mixture was kept at a reduced pressure of −0.07 MPa for 60 min. After being experienced sonication for another 30 min, 2.18 g PMDA was added into the flask to react with ODA by stirring, and then the system was cooled in an ice-water bath and stirred for another 240 min. Secondly, 30 mL DMAc was added into the three-necked flask with stirring for 10 min. Finally, the resultant product was filtered, washed with DMAc, dried at 100°C at reduced pressure (−0.08 MPa) for 8 h, then the PAA/MSNs nanoparticles were gained. The final PI/MSNs nanoparticles were achieved by the thermal imidization of the PAA/MSNs nanoparticles, the corresponding procedures were 80°C for 4 h, 135°C for 2 h, and 300°C for 2 h under air atmosphere.

Preparation of PI/MSNs Nanocomposite Films

Preparation of PI/MSNs nanocomposite films involved two steps, i.e., the synthesis of PAA/MSNs nanocomposite films and the subsequent thermal-imidization of these films. The specific reaction process was depicted in Figure 1. The preparation of PAA/MSNs dispersions for nanocomposite films was consistent with that of PAA/MSNs nanoparticles, which has been described clearly in the previous paragraph. The solid content of the PAA solution was 13 wt %. Then, the PAA/MSNs dispersions with good dispersibility were cast on a glass mould to obtain the films. In order to rapidly remove the solvent, the films were heated at 80°C for 6 h under −0.07 MPa pressure in a vacuum oven. In the second step, these films were thermally handled and the process was carried out at 80°C for 4 h, 135°C for 2 h, and 300°C for 2 h under air atmosphere to get PI/MSNs nanocomposite films. Based on the contents of MSNs in composite films increasing from 0 wt % to 1 wt %, 3 wt %, 5 wt %, 7 wt %, and 9 wt %, the corresponding PI/MSNs nanocomposite films were denoted as PI/MSNs-0, PI/MSNs-1, PI/MSNs-3, PI/MSNs-5, PI/MSNs-7, and PI/MSNs-9, respectively. For comparison, the PI/MSNs-5-I nanocomposite film was prepared strictly according to the above method without the manipulation of keeping the mixture in vacuum (−0.07 MPa) for 60 min. Namely, after the ODA was dissolved completely, the MSNs was just dispersed in the solution with sonication at the normal pressure for 60 min .

Characterizations

The nitrogen adsorption and desorption isotherm was measured at 77 K using a Micromeritics ASAP2020 system. Before the adsorption measurements, the samples were degassed under vacuum at 350°C for 4 h. The pore size distribution was analyzed by Barrette Joynere Halenda (BJH) method. Transmission electron microscopy (TEM, JEOL JEM-2010, Japan) was used to observe the morphologies and microstructures of the prepared MSNs. Energy-dispersive spectrum (EDS) was performed at the acceleration voltage of 200 kV. Field-emission scanning electron microscopy (FE-SEM, JEOL JSM-6701F, Japan) performed at an acceleration voltage of 5.0 kV was employed to observe the morphologies and dispersion state of the MSNs and the fractured surfaces of the pure PI as well as its nanocomposite film samples. Mechanical properties of the films were evaluated by using an universal testing machine (AGS-X 5 KN, Shimadzu, Japan) with a stretched speed of 20 mm min^{-1} at 25°C and 25% relative humidity, and each data point was averaged after five measurements. The transmittance spectrum of the films was scanned from 300 nm to 1300 nm at an interval of 1 nm with an UV–visible spectrophotometer (UV2600, Shimadzu, Japan). Thermo gravimetric analysis (TGA, STA 449C, Germany) was performed under air flow at a heating rate of 10°C min^{-1} from 50°C to 850°C. The glass transition temperature (T_g) data were performed using a Differential Scanning Calorimetry (DSC) Instrument (STA 449C, Germany) from 35 to 450°C in flow nitrogen at the programmed heating rate of 10°C/min.

RESULTS AND DISCUSSION

Morphologies and Microstructures of the Prepared MSNs

The morphologies and microstructures of the obtained mesoporous silica sample were clearly revealed by FE-SEM and TEM. As shown in Figure 2, the results of FE-SEM were almost consistent with that of TEM, and the synthesized mesoporous silica particles were regularly spherical and monodisperse with the

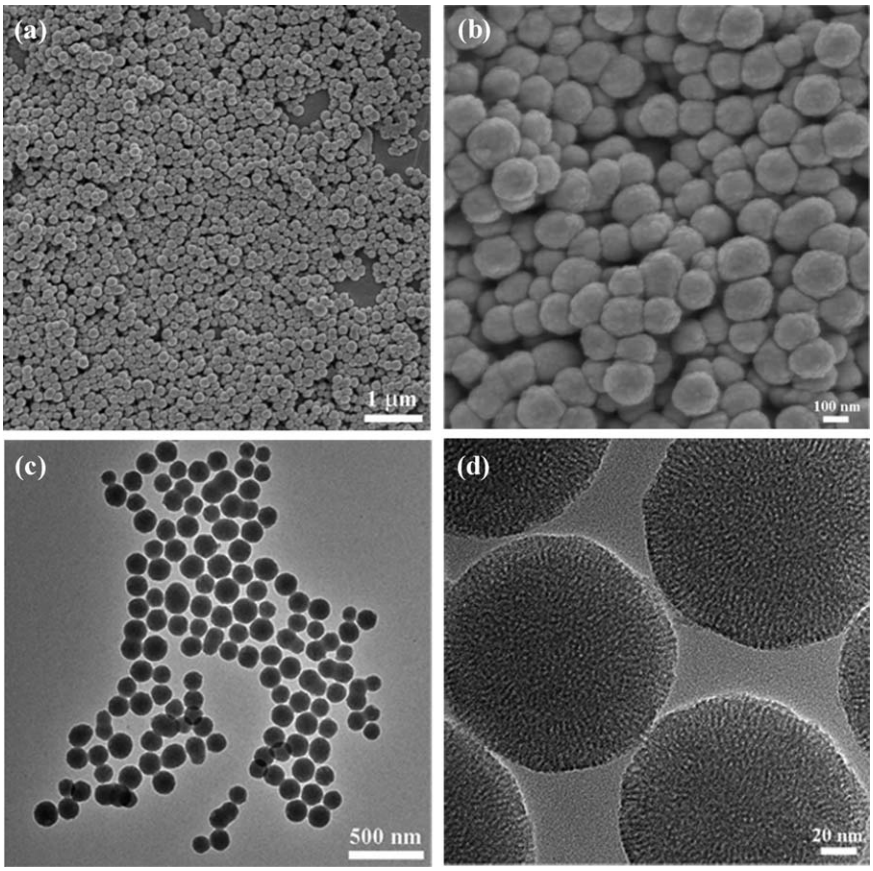

Figure 2. (a) Low- and (b) high-magnification FE-SEM images of the as-prepared MSNs, (c) low- and (d) high-magnification TEM images of the as-prepared MSNs.

uniform diameter of about 150 nm. In addition, it was apparent based on Figure 2(d) and the high resolution TEM images of the MSNs (see Supporting Information Figure S1) that the surface of the sample was smooth and the mesopores of spheres were radically oriented.

The nitrogen adsorption and desorption behavior of the prepared MSNs particles was investigated. The nitrogen sorption isotherm and pore size distribution of the sample were displayed in Figure 3 (a). Apparently, the isotherm can be classified as the type IV isotherm according to the International Union of Pure and Applied Chemistry (IUPAC) nomenclature. Meanwhile, it can be found that capillary condensation inside the mesopores caused a steep increase of absorbed volume at the relative pressure of $0.21 < p/p_o < 0.35$. The long plateau occurred at the pressure of $0.35 < p/p_o < 0.87$ indicated that pore-filling was restricted to the inflection point at higher

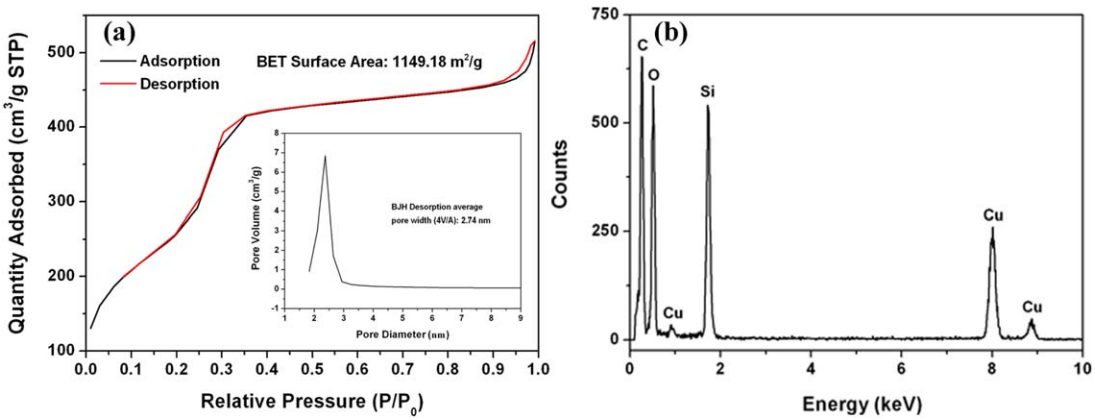

Figure 3. (a) Nitrogen adsorption and desorption isotherm obtained at −196°C and pore size distribution of the as-prepared MSNs after calcination at about 550°C for 5 h, (b) the EDS of the as-prepared MSNs. [Color figure can be viewed in the online issue, which is available at wileyonlinelibrary.com.]

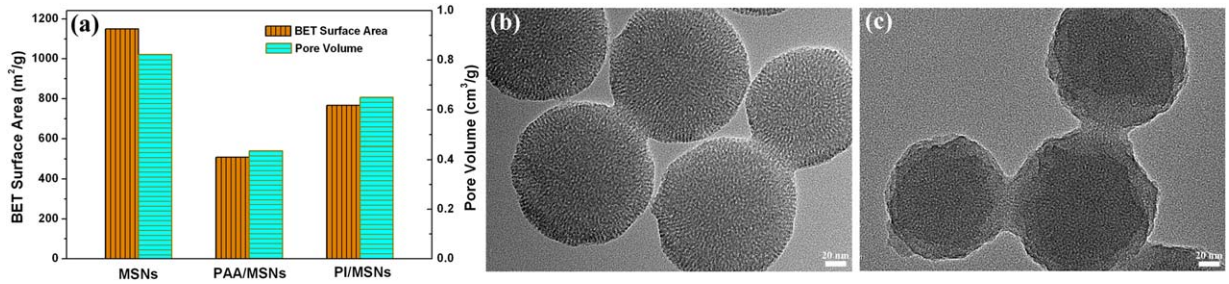

Figure 4. (a) BET surface area and pore volume of MSNs, PAA/MSNs nanoparticles and PI/MSNs nanoparticles; high-magnification TEM images of (b) MSNs and (c) PI/MSNs. [Color figure can be viewed in the online issue, which is available at wileyonlinelibrary.com.]

relative pressures. It should be noted that an adsorbed hysteresis loop appeared at the relative pressure of $0.87 < p/p_o < 0.99$, which meant that nitrogen adsorption and desorption behavior occurred again. At the same time, the inserted figure showed the pore size distribution which was evaluated by the BJH method, indicating that the sample had a narrow pore size distribution and the average pore width was about 2.74 nm. Besides, only the elements of C, O, Si, and Cu can be detected on the EDS and the elements of C and Cu were from the substrate, as clearly shown in Figure 3(b). The EDS further demonstrated that the prepared material was pure silica. In a word, the above measurements revealed that the sample was mesoporous silica with the BET surface area of 1149.18 $m^2 \cdot g^{-1}$.

Morphologies and Microstructures of the Prepared PAA/MSNs and PI/MSNs Nanoparticles

In order to confirm the real achievement of controlling polymerization in the pores of MSNs, the variations of BET surface area and pore volume for samples of MSNs, PAA/MSNs nanoparticles, and PI/MSNs nanoparticles were investigated in virtue of the nitrogen adsorption and desorption isotherms. As displayed in Figure 4(a), the results indicated that the BET surface areas and pore volumes were, respectively, 1149.18 $m^2 \cdot g^{-1}$ and 0.82 $cm^3 \cdot g^{-1}$ for MSNs, 508.89 $m^2 \cdot g^{-1}$ and 0.44 $cm^3 \cdot g^{-1}$ for PAA/MSNs, 766.44 $m^2 \cdot g^{-1}$, and 0.65 $cm^3 \cdot g^{-1}$ for PI/MSNs. According to the previous report,[37] the above significant reduction originated from the impregnation of ODA and PMDA in the pores of MSNs and the subsequent polymerization in the pores. Meanwhile, there were obvious changes in microstructures of MSNs and PI/MSNs nanoparticles, further demonstrating that polymerization occurred in the pores of MSNs. Compared the high-magnification TEM images of MSNs [Figure 4 (b)] with PI/MSNs [Figure 4(c)], two obvious features can be found. First and foremost, the total number of the pores decreased partly, corresponding to the reductions of BET surface area and pore volume of the MSNs after PI polymerized in the pores of the MSNs. Secondly, the contrast between the silica wall and the pore became ambiguous because a polymer chain existed inside the pore and the pore was no longer fully empty. Therefore, polymerization of PI occurred in the pores of MSNs via this simple wet impregnation method could be proved by the variations of BET surface area and pore volume, as well as TEM morphology.

Morphologies of PI/MSNs Nanocomposite Films

FE-SEM observation was carried out in order that the detailed information on the microstructures and morphologies of the prepared hybrid nanocomposite films can be obtained. Figure 5(a) provided the FE-SEM image of the fractured surface of the pure PI film, which presented some large plastic deformation, revealing a typical tough fracture behavior. From Figure 5(b–f), it was apparent that large plastic deformation was still existent when various contents of MSNs were added into PI matrix. Meanwhile, one can easily identify distribution of the MSNs in the composite film according to the clear contrast of these two materials. At the same time, the obvious aggregation of the MSNs can be found with the increase of the MSNs, as clearly displayed in Figure 5(e,f). The similar phenomenon can also be reflected in the UV–visible transmittance spectroscopy. As exhibited in Figure 6, the transmittances for the samples of PI/MSNs-1, PI/MSNs-3, PI/MSNs-5, PI/MSNs-7, and PI/MSNs-9 within the wavelength scope of 300 to 1300 nm were inferior to pure PI, and the transmittance decreased gradually with the increase of the MSNs. The decrease of the transmittance can be boiled down to the addition of MSNs because the MSNs can cause light scattering; meanwhile, aggregations of the MSNs will occur with the increase of the MSNs, which can cause more severe light scattering.[38]

Mechanical Properties

Typical stress–strain curves of pure PI and PI/MSNs nanocomposite films were presented in Figure 7(a), and the corresponding Young's modulus and elongation at break of the PI/MSNs nanocomposite films were plotted in Figure 7(b). As expected, the content of the MSNs had a significant effect on the mechanical properties of nanocomposite films. As indicated in Figure 7(a), the tensile stress of the PI/MSNs nanocomposite films increased with continuous increase of MSNs until its concentration reached 5 wt %, and then began to decrease. Figure 7(b) revealed Young's modulus of the PI/MSNs nanocomposite films increased rapidly by adding the MSNs and then increased slowly when the concentration exceeded 5 wt %. At the same time, elongation at break of the PI/MSNs nanocomposite films decreased gradually with the increase of the MSNs.

Here, the above remarkable characteristics of the PI/MSNs nanocomposite materials should be attributed to the polymerization occurred in the pores of the MSNs. For the sake of further demonstrating polymerization in the pores of the MSNs plays a crucial role in improving the mechanical strength of the PI/MSNs nanocomposite films, and the mechanical properties between the PI/MSNs-5 and the PI/MSNs-5-I were tested and compared. As shown in Figure 8, the tensile stress of 97.65 MPa

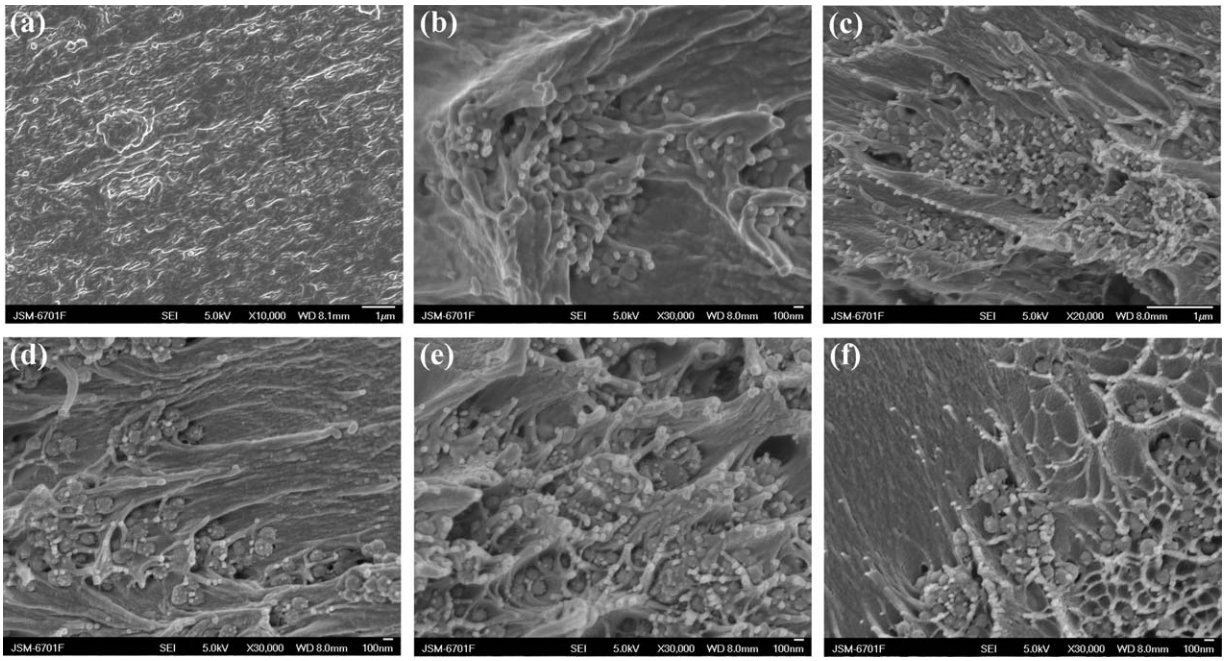

Figure 5. Fractured surface morphologies of the PI/MSNs nanocomposite films: (a) PI/MSNs-0, (b) PI/MSNs-1, (c) PI/MSNs-3, (d) PI/MSNs-5, (e) PI/MSNs-7, and (f) PI/MSNs-9.

for the PI/MSNs-5 is apparently higher than that of 69.46 MPa for the PI/MSNs-5-I. Actually, Lee et al.[35] also studied the tensile stress of PI/mesoporous silica nanocomposite films; nevertheless, they found that tensile modulus of the nanocomposite films were lower than the pure PI; however, when the content of mesoporous silica was 5%, the tensile modulus of 60.9 MPa for the nanocomposite film was comparable with the value of 69.46 MPa for this PI/MSNs-5-I.

The polymerization occurred in the pores of the MSNs was undertaken to explain the improvements of mechanical properties. Actually, there were several groups had already actualized the polymerization of polymers (e.g., polystyrene and polymethyl methacrylate) inside the pores of mesoporous silica.[39,40] Especially, Cheng et al.[39] had validated polymerization of polyimide (ODPA-BAPP) in the pores of nanoscale mesoporous silica (NMS) modified by 3-aminopropyltrimethoxysilane (APTMS), and the covalent bond is dominant in the improvements of the mechanical properties and the thermal stability of polyimide (ODPA-BAPP). Here, our experimental results sufficiently illustrated that polymerization of PI (PMDA-ODA) in the pores of MSNs also can come true, and the mechanical properties and the thermal stability of PI could be really improved by adding the MSNs without any chemical modifications. Therefore, it can be accepted that the molecular chains of PI interpenetrating with the silica framework through the pores of MSNs would form a physically inseparable robust polymer network integrated with the silica framework, which can increase the stability of polymeric system.

Thermal Properties

In order to achieve more practically thermal properties of the prepared nanocomposite films, the effect of the MSNs on the thermal stability of the nanocomposite films was investigated by the use of TGA within the temperature range from 50 to 850°C at air atmosphere. From the TGA curves shown in Figure 9, one can observe that the thermal degradation of the pure PI and its nanocomposite films occurred in this temperature range through one degradation step, indicating that the addition of MSNs into the PI matrix did not have impact on the crystallization and microstructures of PI. It was also evident that water or solvent had been successfully removed from the PI film and its nanocomposite films because no weight loss is visible below 100°C. Moreover, the TGA curves also clearly indicated that the thermal stability of the PI was improved with the increase of the MSNs in terms of the weight residues above 700°C. The inserted picture in Figure 9 illustrated that at the weight

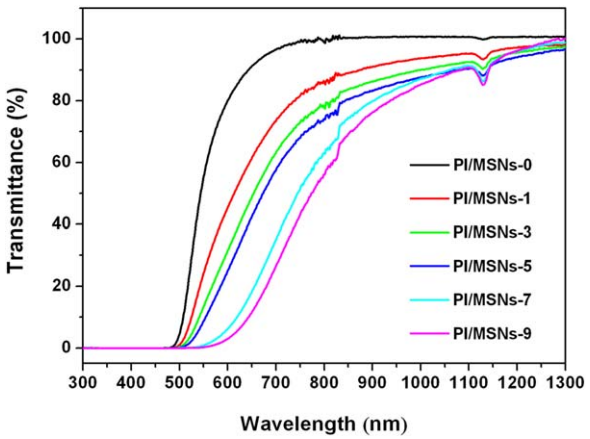

Figure 6. UV–visible transmittance spectroscopy curves of PI/MSNs-0, PI/MSNs-1, PI/MSNs-3, PI/MSNs-5, PI/MSNs-7, and PI/MSNs-9. [Color figure can be viewed in the online issue, which is available at wileyonlinelibrary.com.]

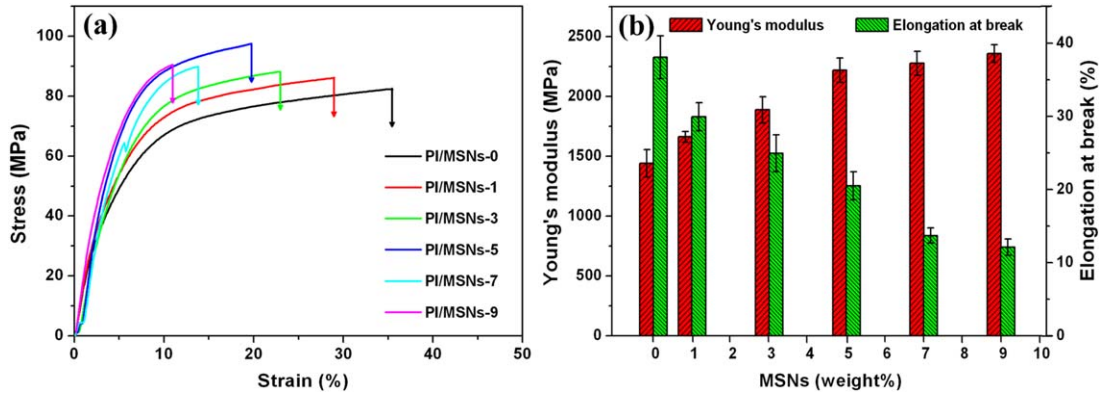

Figure 7. (a) Typical stress–strain curves of pure PI and PI/MSNs nanocomposite films, (b) Young's modulus and elongation at break of the PI/MSNs nanocomposite films as a function of the MSNs' content. [Color figure can be viewed in the online issue, which is available at wileyonlinelibrary.com.]

residues of 20%, the corresponding temperatures were 673°C for PI/MSNs-0, 681°C for PI/MSNs-3, 691°C for PI/MSNs-5, and 697°C for PI/MSNs-7, demonstrating the thermal stability improvement of the nanocomposite films was resulted from the addition of MSNs. That is to say, inorganic components, such as silica, with inherently good thermal stability, can greatly improve the thermal stability of organic materials through forming a cross-linked form between the PI and the silica framework. Meanwhile, the T_g of PI/MSNs nanocomposites increased via adding the MSNs and the T_g data were presented in Supporting Information Figure S2 by the DSC traces. Thereinto, the PI/MSNs-5 has a T_g of 379.6°C, which is apparently higher than that (346.2°C) of the pure PI.

CONCLUSIONS

A simple and feasible method of actualizing polymerization in the pores of mesoporous silica has been developed for the synthesis of PI/MSNs nanocomposite films. First, the MSNs with the diameter of about 150 nm were prepared, and their average pore diameter and BET surface area were 2.74 nm and 1149.18 $m^2 \cdot g^{-1}$, respectively. Then, series of the novel PI (PMDA-ODA) nanocomposite films containing various contents of MSNs were successfully prepared via absorbing ODA and PMDA monomers into the pores of MSNs, following the polymerization and subsequent thermal imidization. The above research indicated two significant results: (1) the polymerization of PI can occur in the pores of MSNs via a simple wet impregnation method; (2) polymerization of PI occurred in the pores of MSNs had an important impact on some properties of the PI/MSNs nanocomposite films. Specially, the tensile stress and Young's modulus of the prepared composite film reached 97.65 MPa and 2220.06 MPa by incorporating 5 wt % of MSNs. Moreover, the thermal stability of PI film was also greatly improved by incorporating a quantity of MSNs, which is due to the fact that the MSNs have inherently good thermal stability. All in all, the polymerization occurred in the pore effectively increased interaction between organic matrix and inorganic nanofillers, which was beneficial to highlight the respective advantages of the two components. Anticipatedly, the nanocomposite materials based on the MSNs and PI prepared from controlling polymerization in the pores may attract much more attention because it is an important and effective means to improve the properties of nanocomposite materials.

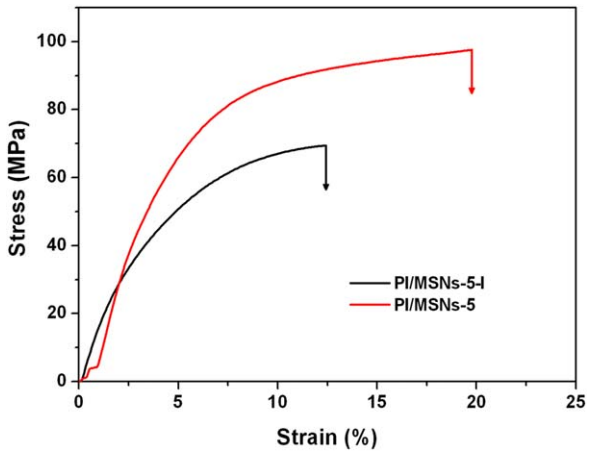

Figure 8. Typical stress–strain curves of PI/MSNs-5 and PI/MSNs-5-I nanocomposite films. [Color figure can be viewed in the online issue, which is available at wileyonlinelibrary.com.]

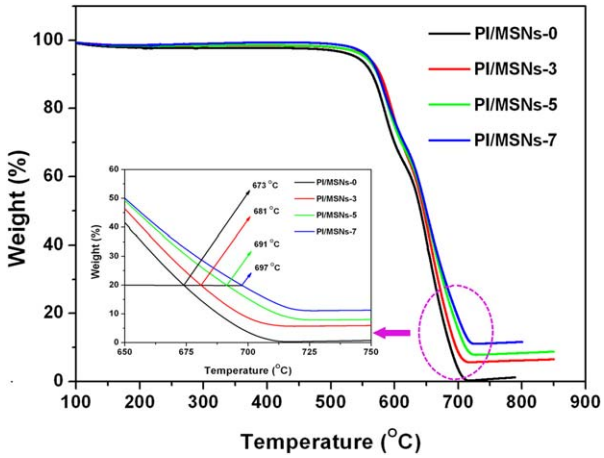

Figure 9. TGA thermograms of the pure PI and its nanocomposite films at air atmosphere. [Color figure can be viewed in the online issue, which is available at wileyonlinelibrary.com.]

ACKNOWLEDGMENTS

This work was supported by the National Natural Science Foundation of China (Grant Nos. 51075384 and 51375474), and the "Funds for Distinguished Young Scientists of Gansu Province" scheme.

AUTHOR CONTRIBUTIONS

Xiangyuan Ye contributed in the experimental design and operation, the acquisition, analysis and interpretation of data, the drafting and revision of the article. Jinqing Wang contributed in the experimental design, the analysis of data, the revision of the article, and submitting the article. Ye Xu contributed in the acquisition, analysis and interpretation of data. Lengyuan Niu contributed in the analysis, interpretation of data, and the revision of the article. Zengjie Fan contributed in the interpretation of data and the revision of the article. Peiwei Gong contributed in the interpretation of data and the revision of the article. Limin Ma contributed in the interpretation of data. Honggang Wang contributed in the interpretation of data and the revision of the article. Zhigang Yang contributed in the analysis of data. Shengrong Yang contributed in the interpretation of data and the revision of the article.

REFERENCES

1. Mark, J. E. *Accounts Chem. Res.* **2006**, *39*, 881.
2. Luonga, N. D.; Hippia, U.; Korhonenb, J. T.; Soininenb, A. J.; Ruokolainenb, J.; Johanssonc, L. S.; Namd, J.-D.; Le Hoang Sinhd, J. S. *Polymer* **2011**, *52*, 5237.
3. Park, O. K.; Hwang, J. Y.; Goh, M.; Lee, J. H.; Ku, B. C.; You, N. H. *Macromolecules* **2013**, *46*, 3505.
4. Ahmad, Z.; Mark, J. *Chem. Mater.* **2001**, *13*, 3320.
5. Moniruzzaman, M.; Winey, K. I. *Macromolecules* **2006**, *39*, 5194.
6. Zou, H.; Wu, S.; Shen, J. *Chem. Rev.* **2008**, *108*, 3893.
7. Wei, L.; Tang, T.; Huang, B. *J. Polym. Sci. Part A: Polym. Chem.* **2004**, *42*, 941.
8. Ma, P.; Nie, W.; Yang, Z.; Zhang, P.; Li, G.; Lei, Q.; Gao, L.; Ji, X.; Ding, M. *J. Appl. Polym. Sci.* **2008**, *108*, 705.
9. Tong, Y.; Li, Y.; Xie, F.; Ding, M. *Polym. Int.* **2000**, *49*, 1543.
10. Zhang, L. B.; Wang, J. Q.; Wang, H. G.; Xu, Y.; Wang, Z. F.; Li, Z. P.; Mi, Y. J.; Yang, S. R. *Compos. Part A: Appl. Sci. Manufac.* **2012**, *43*, 1537.
11. Park, C.; Kim, J. W.; Sauti, G.; Ho Kang, J.; Lovell, C. S.; Gibbons, L. J.; Lowther, S. E.; Lillehei, P. T.; Harrison, J. S.; Nazem, N. *J. Polym. Sci. Part B: Polym. Phys.* **2012**, *50*, 394.
12. Yoonessi, M.; Shi, Y.; Scheiman, D. A.; Lebron-Colon, M.; Tigelaar, D. M.; Weiss, R.; Meador, M. A. *Acs Nano* **2012**, *6*, 7644.
13. WookáKang, S.; HyunáBaik, J. *Polym. Chem.* **2013**, *4*, 290.
14. Liu, L.; Liang, B.; Wang, W.; Lei, Q. *J. Compos. Mater.* **2006**, *40*, 2175.
15. Zhu, B. K.; Xie, S. H.; Xu, Z. K.; Xu, Y. Y. *Compos. Sci. Technol.* **2006**, *66*, 548.
16. Hsiue, G. H.; Chen, J. K.; Liu, Y. L. *J. Appl. Polym. Sci.* **2000**, *76*, 1609.
17. Huang, Y.; Gu, Y. *J. Appl. Polym. Sci.* **2003**, *88*, 2210.
18. Karataş, S.; Kayaman Apohan, N.; Demirer, H.; Güngör, A. *Polym. Adv. Technol.* **2007**, *18*, 490.
19. Kramarenko, V. Y.; Shantalil, T. A.; Karpova, I. L.; Dragan, K. S.; Privalko, E. G.; Privalko, V. P.; Fragiadakis, D.; Pissis, P. *Polym. Adv. Technol.* **2004**, *15*, 144.
20. Li, Y. Q.; Fu, S. J.; Li, Y. Q.; Pan, Q. Y.; Xu, G.; Yue, C. Y. *Compos. Sci. Technol.* **2007**, *67*, 2408.
21. Morikawa, A.; Iyoku, Y.; Kakimoto, M. A.; Imai, Y. *Polym. J.* **1992**, *24*, 107.
22. Musto, P.; Ragosta, G.; Scarinzi, G.; Mascia, L. *Polymer* **2004**, *45*, 1697.
23. Shang, X. Y.; Zhu, Z. K.; Yin, J.; Ma, X. D. *Chem. Mater.* **2002**, *14*, 71.
24. Wang, L.; Tian, Y.; Ding, H.; Li, J. *Eur. Polym. J.* **2006**, *42*, 2921.
25. Babanzadeh, S.; Mehdipour-Ataei, S.; Mahjoub, A. R. *Des. Monomers Polym.* **2013**, *16*, 417.
26. Wang, Z. D.; Lu, J. J.; Li, Y.; Fu, S.; Jiang, S. Q.; Zhao, X. X. *Compos. Part A: Appl. Sci. Manuf.* **2006**, *37*, 74.
27. Liu, H.; Wang, T.; Wang, Q. *J. Appl. Polym. Sci.* **2012**, *125*, 488.
28. Didier, B.; Mercier, R.; Alberola, N. D.; Bas, C. *J. Polym. Sci. Part B: Polym. Phys.* **2008**, *46*, 1891.
29. Zhang, Y. H.; Li, Y.; Fu, S. Y.; Xin, J. H.; Daoud, W. A.; Li, L. F. *Polymer* **2005**, *46*, 8373.
30. Rui, J. M. *Adv. Mater. Res.* **2013**, *716*, 172.
31. Zhang, Y.; Yu, L.; Su, Q.; Zheng, H.; Huang, H.; Chan, H. *J. Mater. Sci.* **2012**, *47*, 1958.
32. Lin B. P.; Tang J. N.; Liu H. J.; Sun Y. M.; Yuan C. W. *J. Solid State Chem.* **2005**, *178*, 650.
33. Lin, J.; Wang, X. *Polymer* **2007**, *48*, 318.
34. Min, C. K.; Wu, T. B.; Yang, W. T.; Chen, C. L. *Compos. Sci. Technol.* **2008**, *68*, 1570.
35. Lee, T.; Park, S. S.; Jung, Y.; Han, S.; Han, D.; Kim, I.; Ha, C. S. *Eur. Polym. J.* **2009**, *45*, 19.
36. Li Z. K.; Xi H. A.; Qian X. F.; Yin J.; Zhu Z. K. *J. Inorg. Mater.* **2003**, *18*, 1102.
37. Yang, S.; Zhan, L.; Xu, X.; Wang, Y.; Ling, L.; Feng, X. *Adv. Mater.* **2013**, *25*, 2130.
38. Huang, Z.; Zhao, J.; Yuan, Y.; Yan, S.; Liu, S.; Zan, X. *Polym. Adv. Technol.* **2013**, *24*, 600.
39. Cheng, C. F.; Cheng, H. H.; Cheng, P. W.; Lee, Y. J. *Macromolecules* **2006**, *39*, 7583.
40. Choi, M.; Kleitz, F.; Liu, D.; Lee, H. Y.; Ahn, W. S.; Ryoo, R. *J. Am. Chem. Soc.* **2005**, *127*, 1924.